Journal of Advanced Research 28 (2021) 231–243

Contents lists available at ScienceDirect

Journal of Advanced Research

journal homepage: www.elsevier.com/locate/jare

# Quercetin alleviates acute kidney injury by inhibiting ferroptosis

Yue Wang [a,1], Fei Quan [a,1], Qiuhua Cao [a], Yanting Lin [a], Chongxiu Yue [a], Ran Bi [a], Xinmeng Cui [a], Hongbao Yang [a], Yong Yang [a,b], Lutz Birnbaumer [c,d], Xianjing Li [a,*], Xinghua Gao [a,*]

[a] Center for New Drug Safety Evaluation and Research, State Key Laboratory of Natural Medicines, China Pharmaceutical University, Nanjing, Jiangsu 211198, PR China
[b] School of Pharmacy, Xuzhou Medical University, 209 Tongshan Road, Xuzhou 221004, Jiangsu, PR China
[c] Neurobiology Laboratory, National Institute of Environmental Health Sciences, Research Triangle Park, NC 27709, USA
[d] Institute of Biomedical Research (BIOMED), Catholic University of Argentina, Buenos Aires C1107AFF, Argentina

## HIGHLIGHTS

- Quercetin (QCT) inhibits ferroptosis but not apoptosis, necrosis or autophagy of renal proximal tubular epithelial cells, and ameliorates AKI induced by ischemia–reperfusion (I/R) or folic acid (FA).
- Activation transcription factor 3 (ATF3) plays an important role in cell ferroptosis, while QCT significantly inhibits the expression of ATF3 and further blocks the downstream signaling pathway of ferroptosis.
- Ferroptotic cells induce the recruitment and chemotaxis of macrophages through CCL2, triggering inflammation and enhancing tissue injury.

## GRAPHICAL ABSTRACT

A proposed model illustrating the therapeutic effect of QCT on AKI. QCT inhibits the expression of ATF3. While ATF3 blocks the system Xc-, and then suppresses GPX4, inducing ferroptosis. In another side, ferroptotic cells secrete chemokines like CCL2, CCL7, induce the recruitment of macrophages, and then cause the inflammation in AKI. In summary, QCT ameliorates AKI through the inhibition on ferroptosis and the following inflammation.*Introduction:*

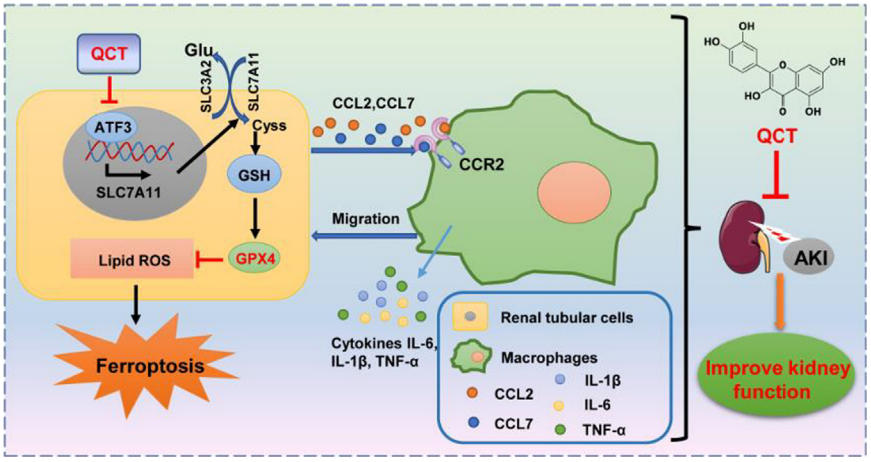


## ARTICLE INFO

*Article history:*
Received 26 March 2020
Revised 18 June 2020
Accepted 16 July 2020
Available online 22 July 2020

*Keywords:*
Ferroptosis
Quercetin

## ABSTRACT

*Introduction:* Ferroptosis is an iron-dependent regulated necrosis and has been proven to contribute to the progress of acute kidney injury (AKI). Quercetin (QCT), a natural flavonoid which is commonly found in numerous fruits and vegetables, has extensive pharmacological effects, such as anti-oxidant, anti-inflammatory and anti-senescence effects.
*Objectives:* This study aims to explain whether ferroptosis is a therapeutic strategy to AKI, and to explore the effect of QCT on AKI ferroptosis.
*Methods:* NRK-52E cells and HK-2 cells were used for in vitro ferroptosis studies. Morphology of cells was detected by transmission electron microscopy. Lipid ROS was assayed using flow cytometry. In vivo, AKI

Peer review under responsibility of Cairo University.

* Corresponding authors.
*E-mail addresses:* xjl@cpu.edu.cn (X. Li), gaoxinghua@cpu.edu.cn (X. Gao).

[1] These authors contributed equally to this work.

https://doi.org/10.1016/j.jare.2020.07.007
2090-1232/

Acute kidney injury
Activation transcription factor 3
Macrophages

was induced by ischemia–reperfusion (I/R) or folic acid (FA). To explore the molecular mechanisms, RNA-sequence analysis was performed. Transwell was used to detect macrophage migration.
*Results:* We discovered that quercetin (QCT), a natural flavonoid, inhibited ferroptosis in renal proximal tubular epithelial cells. QCT blocked the typical morphologic changes of ferroptotic cells by reducing the levels of malondialdehyde (MDA) and lipid ROS and increasing the levels of glutathione (GSH). Moreover, QCT ameliorated AKI induced by I/R or FA. RNA-sequence analysis highlighted activation transcription factor 3 (ATF3), as it was the dominant one among all the 299 down-regulated genes by QCT. Knockdown of ATF3 could significantly increase the levels of SLC7A11, GPX4 and increased the cell viability. In addition, ferroptotic cells were found to be extremely pro-inflammatory by recruiting macrophages through CCL2, while QCT inhibited the chemotaxis of macrophages induced by ferroptosis in AKI.
*Conclusions:* Collectively, these results identify QCT as a ferroptosis inhibitor and provide new therapeutic strategies for diseases related to ferroptosis.


## Introduction

Cell death is crucial for normal development and homeostasis. Regulated cell death causes tissue injury, leading to a wide variety of diseases, including acute kidney injury (AKI). Regulated necrosis includes necroptosis, pyroptosis, necrosis and ferroptosis [1]. Various types of cell death have different induction factors and characterized pathways. Better understanding of the dominant type of cell death is needed to achieve therapeutic strategies of related diseases.

Acute kidney injury is histologically characterized by tubular cell death and inflammation, which are recognized as the precipitating factors [2]. Ferroptosis, an iron- and ROS-dependent form of regulated cell death, was firstly named by Brent R Stockwell in 2012 [3]. It involves a unique constellation of morphological, biochemical, and genetic features, which differs from other kinds of regulated cell death [3]. Ferroptosis has been implicated in multiple physiological and pathological processes, including carcinoma, AKI, neurodegenerative diseases, ischemia/reperfusion injury and T-cell immunity [4]. Of note is that, among all the tissues, kidney seems to be the most sensitive to iron-dependent ferroptosis. Inactivation of the ferroptosis regulator glutathione peroxidase 4 (GPX4) induces acute renal failure by triggering ferroptosis in kidney tubular cells in mice [5]. Also, renal cell carcinomas are particularly susceptible to GPX4-regulated ferroptosis [6]. In line with these previous studies, ferroptosis could directly cause necrosis of renal tubules in models of I/R injury and oxalate crystal-induced AKI [7], and ferroptosis was also proven to be important in nephrotoxic folic acid (FA)–induced AKI [8]. Following up on these observations, ferroptosis stands out as a promising therapeutical target for AKI.

The potent and specific inhibitor of ferroptosis now widely used in vitro is the small molecule ferrostatin-1 (Fer-1). However, despite the overwhelming evidence highlighting the therapeutic uses of Fer-1, the translational aspect of Fer-1 application in the clinic is limited due to its instability in vivo [7,9]. Thus, finding a drug which is more economic and effective is in demand. Quercetin (QCT), a natural flavonoid which is commonly found in numerous fruits and vegetables, is an indispensable part of the diet. QCT comes into the focus of medicinal interest because of its extensive pharmacological effects, such as anti-cancer, anti-viral, anti-oxidant, anti-inflammatory and anti-senescence effects [10–14]. A previous study reported that QCT could selectively kill senescent cells and enhance lifespan in old mice [15]. QCT was also reported to possess protective effect on diabetic nephropathy [16], and even have the ability of iron chelation [17,18]. Another recent publication reported that QCT could protect bone marrow-derived mesenchymal stem cell from erastin-induced ferroptosis, possibly through the antioxidant pathway [19]. In spite of the attention QCT drew and the wide effects already discovered, the effect of QCT on AKI ferroptosis remains undescribed. In this study, we explored a strong inhibition of QCT on ferroptosis and proved QCT as a promising drug candidate for the treatment of AKI.

## Materials and methods

### Cell lines

NRK-52E Cells were a gift from Dr. Chunsun Dai, and HK-2 cells were obtained from China Cell Bank. Both cells were maintained in DMEM/Ham's F12 (BI) supplemented with 5% fetal bovine serum (BI). Bone marrow derived macrophages (iBMDM) cells were a gift from Dr. Feng Shao, and were cultured with DMEM (Gibco) supplemented with 5% fetal bovine serum (Gibco) and 100 units per ml penicillin and 100 μg/ml streptomycin. All the cells were cultured in 37 °C incubator with 5% $CO_2$.

### Cell viability assay

For cell viability assay, cells were seeded into 96-well plates at a density of $0.8 \times 10^4$ cells per well. Cell viability was measured using the sulforhodamine B (SRB) assay, as previously described [20,21].

### Transmission electron microscopy

Transmission electron microscopy was performed using standard procedures by Wuhan biotechnology. Briefly, cells were fixed with electron microscope fixing solution for 2–4 h. Then cells were embedded with 1% agarose, dehydrated, and cut to ultrathin sections (60–80 nm) with ultramicrotome (Leica UC7, Leica). Sections were stained with uranyl acetate in pure ethanol for 15 min, then stained with lead citrate for 15 min. Images were acquired with Transmission Electron Microscope (HT7700, HITACHI). At least 10 images were acquired for each structure of interest and representative images are shown.

### Lipid ROS assay using flow cytometer

Lipid ROS levels were determined using BODIPY-C11 dye (Invitrogen, cat# D3861) as previously reported [22,23]. The intensely fluorescent BODIPY® (4,4-difluoro-3a,4a-diaza-s-indacene) fluorophore is intrinsically lipophilic, unlike most other long-wavelength dyes. Binding of BODIPY fatty acids to bovine serum albumin can be monitored by the accompanying fluorescence quenching caused by charge-transfer interactions with aromatic amino acid residues. BODIPY 581/591C 11 can be used to measure antioxidant activity in lipid environments by exploiting its loss of fluorescence upon interaction with peroxyl radicals. The cells ($1 \times 10^5$) were treated with Era or RSL3, with or without QCT or

Fer-1 for 24 h. Before the end of time, culture media was replaced with 1 ml media containing 5 μM of BODIPY-C11 dye for 60 min. Cells were harvested and washed twice with PBS followed by re-suspending in 500 μl of PBS. The cell suspension was filtered through cell strainer (70 μm) and subjected to the flow cytometry analysis to examine the amount of ROS within cells. Cells were analyzed with the Invitrogen™ Attune™ NxT Flow Cytometer (Invitrogen, USA) and were calculated using the FlowJo Software.

*Drug treatment*

In vitro experiments: the following reagents were used at the indicated concentrations: Erastin (Era) (MedChemExpress, cat number: HY-15763) (1 μM) and RSL3 (MedChemExpress, cat number: HY-100218A) (0.5 μM) for all experiments. QCT (10 μM) or Fer-1 (1 μM) (Aladdin, cat number: Q111273 or F129882, respectively) was added at the same time with Era or RSL3. The cell death inducers were brefeldin A (Bre-A) (1 μM) (Aladdin, cat number: B102375), hydrogen peroxide ($H_2O_2$) (0.5 mM) (Aladdin, cat number: H112517) and rapamycin (Rapa) (1 μM) (Aladdin, cat number: S115842). RS102895 hydrochloride (RS102895), (MedChemExpress, cat number: HY-18611) 20 μM was added to iBMDMs to the top chamber. In vivo experiments: the dosage of drugs was QCT (25 mg/kg), Fer-1 (5 mg/kg), RS102895 (2.5 mg/kg) and FA (200 mg/kg) separately. QCT was orally gavaged for three times/-day. The solvents for QCT and Fer-1 in vivo were 0.5% CMC-Na and 0.5% DMSO respectively.

*Mice*

Male C57BL/6J mice (20–22 g, 7–8 week) were used for all studies. Mice were housed in a room with a 12 h/12 h light/dark cycle, and habituated in the room 3 days before experiments. All animal experiments were performed in accordance with the National Institutes of Health Guide for the Care and Use of Laboratory Animals, with the approval of Center for New Drug Safety Evaluation and Research, China Pharmaceutical University.

## Animal model

*Renal ischemia /reperfusion model*

Renal ischemia was induced in male mice according to the previous reports [24,25]. Before operation, the drug QCT or Fer-1 was administered. Mice were anesthetized to expose the both kidneys through flank incision. Then mice were kept on a homeothermic plate to induce ischemia for 30 min by clamping the renal pedicle with nontraumatic clamps. Sham groups were subjected to sham operation without induction of ischemia. Blood samples were collected at the time of euthanasia. After reperfusion for 24 h, all the mice were sacrificed. One kidney was fixed in 4% phosphate-buffered formaldehyde for histological analyses, and the other one was snap frozen for subsequent molecular analysis.

*Acute folic acid nephropathy model*

Folic acid nephropathy, a classic model of kidney tubulointerstitial injury and inflammation, was induced by a single i.p. injection of FA (200 mg/kg) in 0.3 mol/L sodium bicarbonate as reported previously [8]. All the mice were euthanized 24 h after drug treatment. Blood samples were collected at the time of euthanasia. One kidney was fixed in 4% phosphate-buffered formaldehyde for histological analyses, and the other one was snap frozen for subsequent molecular analysis.

*Detection of MDA and GSH levels in cell and kidney tissue samples*

Individual levels of MDA and GSH in cell and kidney tissue were measured using MDA and GSH activity assay kits respectively according to the manufacturer's protocol. Individual contents of MDA and GSH were measured at 450 and 405 nm, respectively, with a microplate fluorometer. Total protein concentration was measured using the Bradford method (Beyotime Institute of Biotechnology, Haimen, China).

*Renal function, histology and immunohistochemistry*

Serum creatinine and BUN were determined to monitor renal function as previously described [26,27]. Kidney sections (5 μm) were stained with hematoxylin & eosin (H&E). Tubular injury was evaluated by a pathologist in a blinded manner and was scored based on the degree of damage, as previously described [7,8]. Brush border loss, vacuolization, cell desquamation, tubule dilatation, and tubule degeneration were all scored from 0 to 3, and then all scores were added to yield the tubular injury score, which had a maximal value of 15. Images were obtained with an Olympus BX41 microscope.

*Masson stain of kidney tissue*

Tubular injury in kidney sections was evaluated after Masson staining by a pathologist who was blinded to the nature of the samples. Evidence of cell injury (loss of brush border or vacuolization), cell desquamation, and tubular dilation and signs of regeneration were scored on a semiquantitative zero to three scale, and results from each item were added to yield the tubular injury score, which had a maximal value of 18 [8].

*Iron measurements*

Cells ($2 \times 10^6$) were rapidly homogenized in iron assay buffer with iron assay kit (sigma Aldrich, cat number: MAK025) as previously described [28]. Briefly, iron is released by the addition of an acidic buffer. Samples were tested to measure total iron ($Fe^{2+}$ and $Fe^{3+}$). Released iron could react with the iron probe resulting in a colorimetric (593 nm) product, proportional to the iron present. Then the solution was centrifuged at 13,000*g* for 10 min at 4 °C to remove insoluble material and was measured at 593 nm with a microplate fluorometer.

*Real time PCR analysis*

Total RNA from tissues or cells were extracted using Trizol (Invitrogen), and reverse transcribed into cDNA using a cDNA synthesis kit (Takara). Quantitative PCR was done with a Step one plus Real-Time PCR system (Applied Biosystems, USA) with gene-specific primers. The amount of RNA was calculated by the comparative threshold cycle method. All primers were custom-made by Genscript. The primer sequences are shown in supplementary Table 1.

*RNA-Seq Profiling*

RNA-Seq Profiling was performed by Novogene. Briefly, the cells were treated with Era (1 μM) with or without QCT (10 μM) for 24 h in the incubator. Then the RNA was isolated using the Trizol reagent. A total amount of 3 μg RNA per sample was used as input material for the RNA sample preparations. Sequencing libraries were generated using NEBNext® UltraTM RNA Library Prep Kit for Illumina® (NEB, USA) following manufacturer's recommendations and index codes were added to attribute sequences to each

sample. Briefly, mRNA was purified from total RNA using poly-T oligo-attached magnetic beads. First strand cDNA was synthesized using random hexamer primer and M-MuLV Reverse Transcriptase. Second strand cDNA synthesis was subsequently performed using DNA Polymerase I and RNase H. PCR products were purified (AMPure XP system) and library quality was assessed on the Agilent Bioanalyzer 2100 system. Gene Ontology (GO) enrichment analysis of differentially expressed genes was implemented by the clusterProfiler R package, in which gene length bias was corrected. ClusterProfiler R package was used to test the statistical enrichment of differentially expressed genes in KEGG pathways. Transcripts expression with $|\text{Log2 Fc}| > 1.5$, adjusted P value $< 0.05$ were deemed statistically significant. All genes detected are shown in supplementary file.

*Western blotting*

Briefly, protein samples were boiled for 5 min, electrophoresed in 10% SDS polyacrylamide gel, and transferred onto PVDF membranes (Millipore, Billerica, MA, USA). The blots were blocked with 5% skimmed milk in Tris-buffered saline–Tween 0.1% for 1 h at room temperature and probed with GPX4 (Abcam, cat number: ab125066, 1:2000) or ATF3 (Abcam, cat number: ab58668, 1:1000) primary antibody at the appropriate dilutions over night at 4 °C. The blots were washed and incubated for 1 h at room temperature with the HRP-conjugated secondary antibody, then developed with enhanced chemiluminescence reagents (Millipore). The densitometry of protein bands was quantified using Image J software (National Institutes of Health, Bethesda, MD, USA).

*Transfection*

For transfection of siRNAs, cells were cultured on plates for 24 h and then transfected with ATF3 siRNA (GenePharma, China), or Control siRNA (GenePharma, China) using jetPRIME transfection reagent (Polyplus, Lot#16Y0304K4) according to a protocol provided by the manufacturer.

*Cell migration assay*

The 52E cells ($2 \times 10^5$) were seeded into the bottom chamber of an 8 μm pore transwell insert (Corning, NY) in a 24-well plate, while iBMDMs ($5 \times 10^4$) were seeded into the top chamber. Era or DMSO was added to the bottom chamber for 24 h. Then the chambers were fixed with 4% paraformaldehyde and stained with 0.1% crystal violet to stain the migrated iBMDMs. Images were taken using a Leica DMI 3000B microscope. Number of cells migrated was counted using image J.

*Statistical analysis*

Data are presented as mean ± SEM. Statistical significance was determined by Student's *t* test between two groups, and one-way ANOVA when groups were more than two. $P < 0.05$ was considered statistically significant.

## Results

*QCT inhibited renal tubular cell ferroptosis*

The recognition of ferroptosis as a unique form of regulated cell death emerged from characterizing the lethal mechanism of action of Era and RSL3, which could inhibit the cystine/glutamate antiporter or GPX4 respectively [3,29]. We then firstly treated NRK-52E cells (52E Cells) and HK-2 cells with Era or RSL3 to induce ferroptosis. Intriguingly, QCT abolished cell death induced by Era or RSL3 in 52E cells or HK-2 cells, just as Fer-1 did, which is a selective inhibitor of ferroptosis (Fig. 1A, Fig S1A). As ferroptosis coincided with morphologic changes, transmission electron microscopy studies revealed that QCT or Fer-l could significantly protect Era-induced mitochondrial cristae disappearance and outer membrane rupture in 52E cells (Fig. 1B). As lipid peroxidation is a character of ferroptosis, we next determined the lipid-associated products and ROS of cells. MDA and GSH serve key roles in maintaining the balance of oxidation and reduction. Along with the increase of MDA induced by Era, a decrease of GSH was observed in both 52E and HK-2 cells. Consistently, QCT or Fer-1 blocked the effects of Era on MDA and GSH (Fig. 1C). Furthermore, treatment of 52E cells with Era or RSL3 resulted in an increase in lipid ROS, while incubation with QCT or Fer-1 terminated the increase of lipid ROS (Fig. 1D, E). These were also confirmed in HK-2 cells as shown in Fig. S1B. Remarkably, QCT could not rescue the cell viability in Bre-A-induced apoptosis, $H_2O_2$-induced necrosis, or Rapamycin-induced autophagy in both 52E and HK-2 cells (Fig. S1C, D). These results suggest QCT was a selective ferroptosis inhibitor.

*QCT protects the kidney in both I/R and FA induced AKI*

According to previous reports, ferroptosis of renal tubular cells contributes significantly to the process of AKI [7,8]. Based on the potent inhibitory effect of QCT on ferroptosis, we explored the possible role of QCT in AKI. QCT itself did not have an effect on normal mice, including kidney coefficient and the levels of blood urea nitrogen (BUN) and blood creatinine (CRE) (Fig. S2A). The experimental procedure of I/R induced AKI and administration of drugs is depicted in schematic diagram (Fig. 2A). QCT displayed a protective role by reducing kidney coefficient and the content of BUN and CRE in I/R-AKI (Fig. 2B). Tubular injury was evaluated in kidney sections by Masson staining (Fig. 2C) and HE staining (Fig. S2B), which showed that QCT significantly reduced histologic injury. To confirm these findings, we performed another AKI model using FA (Fig. 2D). Consistently, QCT protected the functional acute renal failure (Fig. 2E) and structural organ damage (Fig. 2F and Fig. S2C) in mice of FA-induced AKI model. Lipid peroxidation in kidney tissues was measured by levels of GSH and MDA. QCT increased the level of GSH and reduced MDA content in the kidney of both AKI models (Fig. 2G). Immunofluorescence staining of kidney tissue section showed QCT reduced kidney cell death with TUNEL assay kit (Fig. S2D). Together, these data support the hypothesis that QCT is a promising drug candidate for treatment of AKI by inhibiting ferroptosis of tubular epithelial cells

*The inhibitory effect of QCT on ferroptosis was depended on the repression of ATF3*

Next, we embarked to decipher the molecular mechanisms that may account for the QCT's inhibition of ferroptosis. As ferroptosis is dependent upon intracellular iron and occurs due to lipid peroxide accumulation, we first determined the influence of QCT on intracellular iron levels and expression of acyl-CoA synthetase long-chain family member 4 (ACSL4), which is an essential component for lipid peroxide accumulation [30]. No obvious differences of intracellular iron and expression levels of *ACSL4* mRNA were found in all groups (Fig. 3A, B). We then explored the antioxidant defenses of the cell, and results revealed a dramatic decrease of GPX4 mRNA and protein accompanied by ferroptosis, while QCT rescued the defective expression (Fig. 3C, D). To further explore the molecular mechanisms, we performed 52E cell RNA-sequence analysis. Compared with Era group, activation transcription factor 3 (ATF3) was predominately low among all the down-regulated genes, while SLC7A11, a subunit unique to system $Xc^-$, was higher

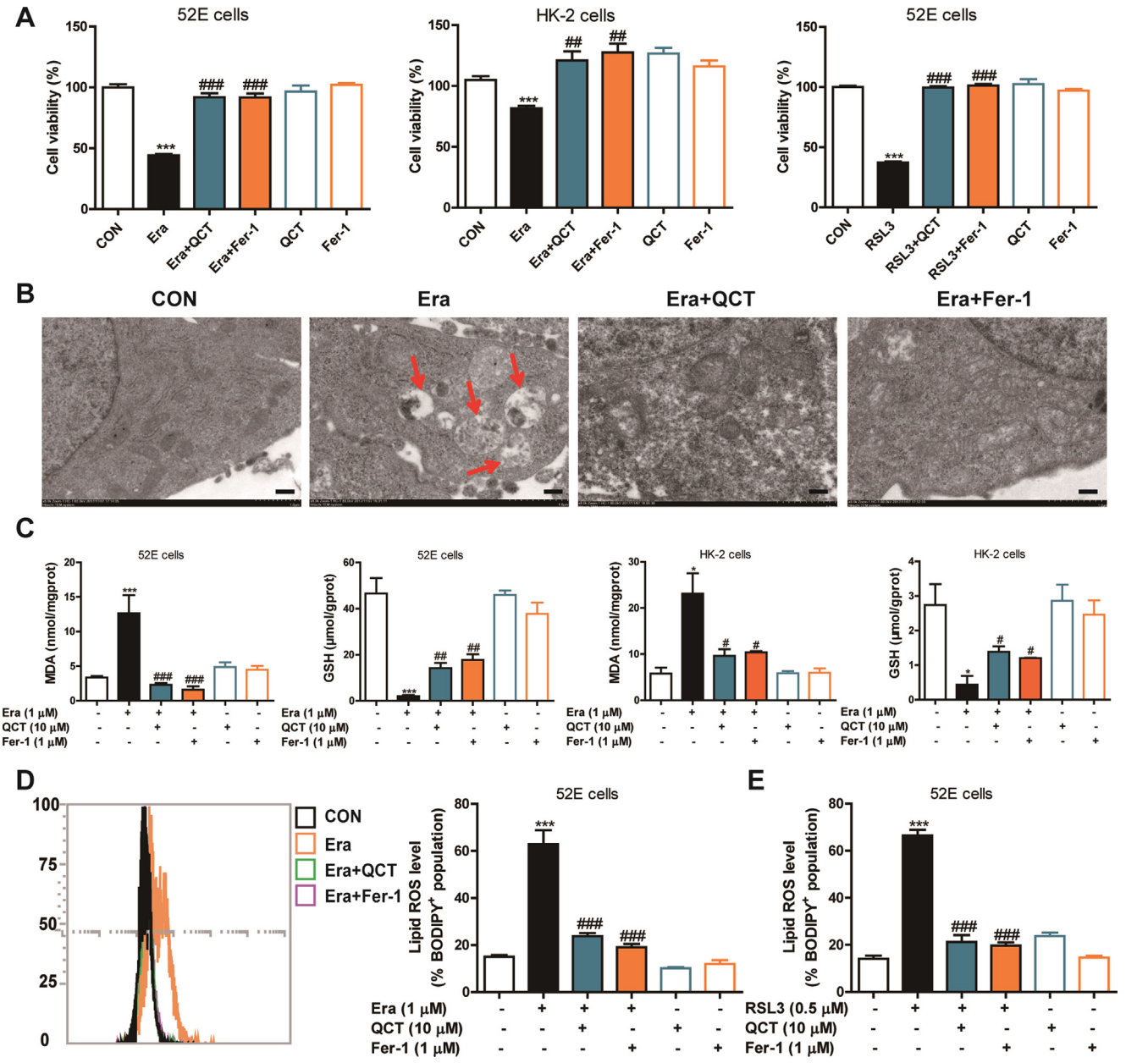


**Fig. 1.** QCT significantly and specially inhibited ferroptosis in 52E and HK-2 cells. **(A)** Cell viability assayed by SRB. (n = 6). The cells were treated with drugs for 24 h. **(B)** Representative pictures acquired by transmission electron microscopy. Red arrows indicated mitochondrial cristae disappearance and outer membrane rupture. The 52E cells were treated for 24 h with Erastin (Era, 1 μM) with or without QCT (10 μM) or Fer-1 (1 μM). The scale bar represents 1 μm. **(C)** MDA and GSH levels in 52E and HK-2 cells. (n = 3). The cells were treated for 24 h. **(D) and (E)** The 52E cells were treated with indicative drugs for 24 h and lipid ROS level was assayed by flow cytometry using C11-BODIPY. (n = 3). *$P$ < 0.05, ***$P$ < 0.001, compared with normal group; #$P$ < 0.05, ##$P$ < 0.01, ###$P$ < 0.001, compared with Era or RSL3 group.

in the QCT treated group (Fig. 3E). Enrichment analysis revealed that QCT-changed genes were correlated with the glutathione metabolic pathway (Fig. 3F). PCR results also confirmed QCT could upregulate the levels of on *SLC7A11* and *SLC3A2*, and downregulate the levels of *ATF3* as well as *Heme Oxygenase 1 (Hmox-1)* (Fig. 3G). To elucidate whether impaired expression of ATF3 was responsible for the inhibition of ferroptosis, we knocked down the expression of ATF3 with siRNA, and the knockdown efficiency was confirmed both at the mRNA and protein levels as shown in Fig. 3H. Interestingly, knockdown of ATF3 significantly increased the expression of SLC7A11 and GPX4, while it decreased the lipid ROS levels, and resulted in an increase of cell viability (Fig. 3I). These results suggest that the ATF3 block by QCT may contribute to its inhibition on ferroptosis.

The mechanism of action of QCT was confirmed in vivo. Similar to the in vitro studies, QCT had no effect on levels of *ATF3* and *Hmox1* in normal mice, but significantly decreased the levels *of ATF3* as well as *Hmox-1* in mice subjected to the I/R-AKI model (Fig. 4A, B, Fig. S4A, B). The mRNA and protein levels of GPX4 were not influenced by QCT in normal mice (Fig. S4B, C). But they were diminished in the I/R group and were significantly restored after QCT treatment (Fig. 4B, C). In accordance with the I/R-AKI model, all the results were repeatable in mice of the FA-AKI model (Fig. 4-D-F). In addition, no obvious iron accumulation was found in all groups in both models (Fig. S3A, B). These in vivo findings fit well with in vitro evidence that QCT inhibits ferroptosis through the reduction of ATF3.

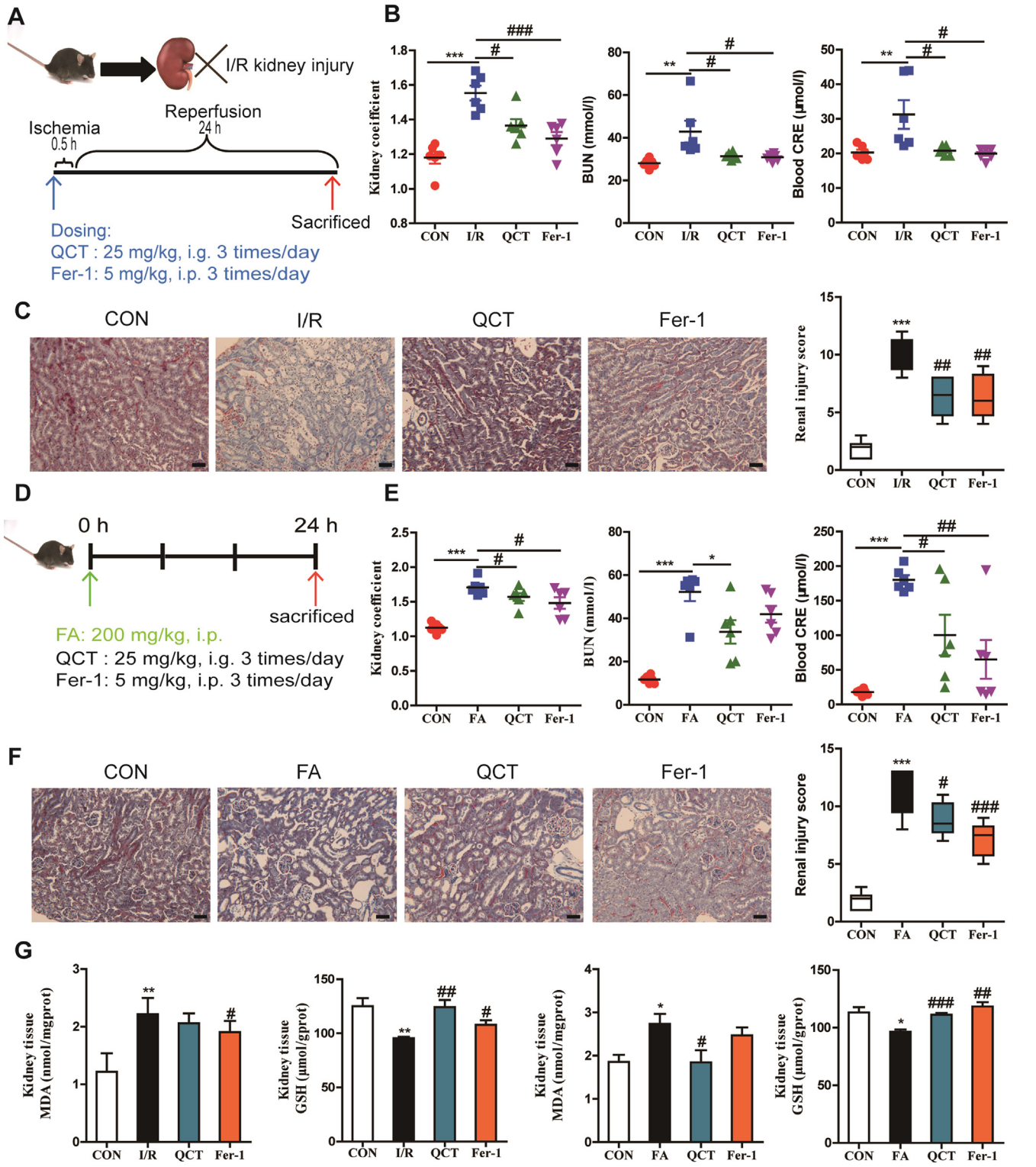


**Fig. 2.** QCT possessed the protective effect to the kidney in both I/R and FA induced AKI. QCT or Fer-1 was administrated 3 times/day, first at the time of model induction, and then 8 h intervals. **(A)** The scheme of I/R-induced AKI model and drug treatment. **(B)** Kidney coefficient and BUN and blood CRE levels in I/R-AKI mice. Kidney coefficient = Kidney weight/body weight × 100. **(C)** Representative Masson staining, and pathological scores of the kidney in I/R-AKI groups. The scale bar represents 50 μm. **(D)** The scheme of FA-induced AKI model and drug treatment. **(E)** Kidney coefficient and BUN and blood CRE levels in FA-AKI mice. Kidney coefficient = Kidney weight/body weight × 100. **(F)** Representative Masson staining, and pathological scores of the kidney in FA-AKI groups. The scale bar represents 50 μm. **(G)** MDA and GSH levels in kidney tissues in both I/R-AKI and FA-AKI groups. (n = 6). $^{*}P < 0.05$, $^{**}P < 0.01$, $^{***}P < 0.001$, compared with Control (CON) group; $\#P < 0.05$, $\#\#P < 0.01$, $\#\#\#P < 0.001$, compared with I/R or FA group.

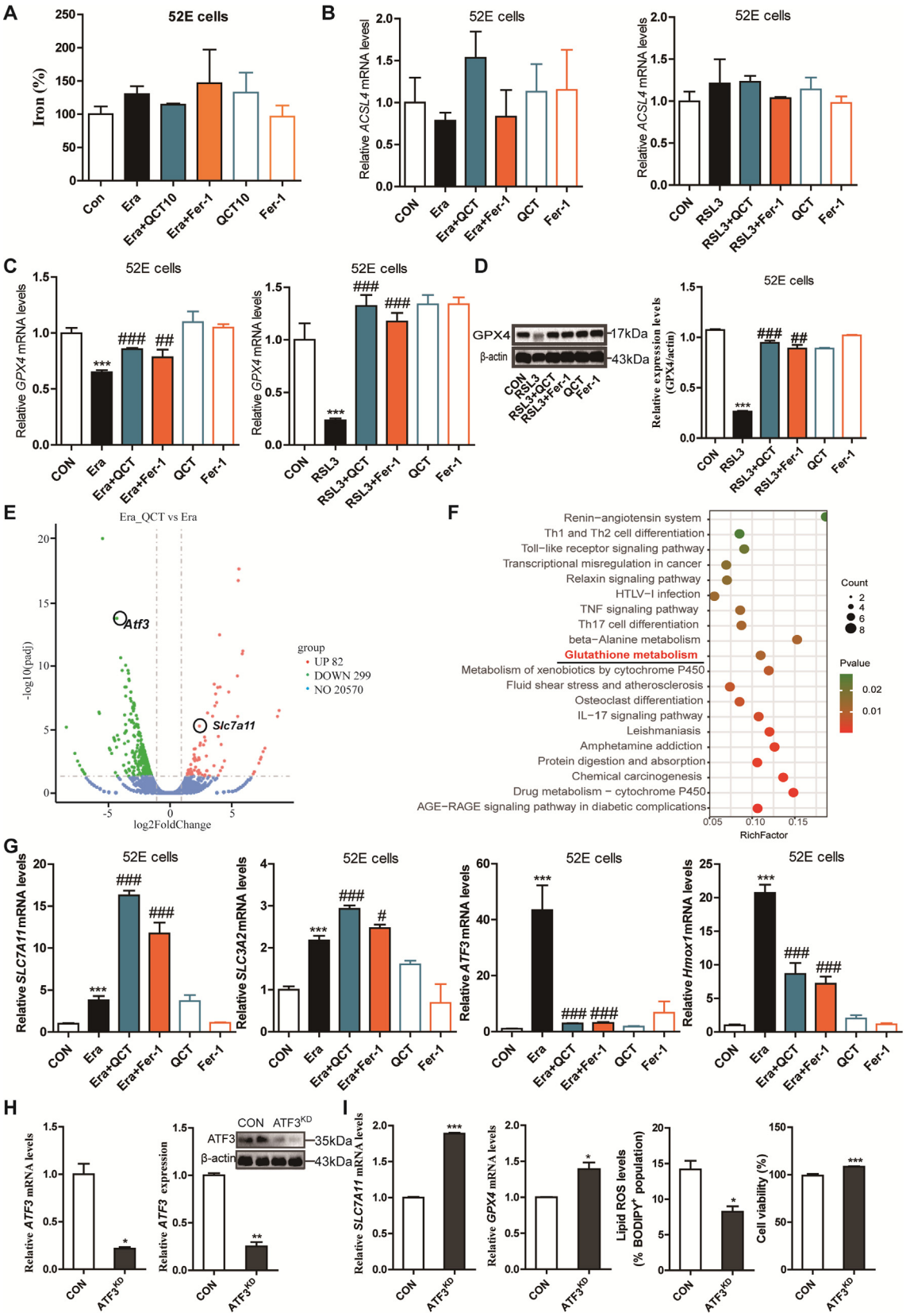


**Fig. 3.** Inhibitory effect of QCT on ferroptosis was depended on the repression of ATF3. The cells were treated with drugs as indicated ahead for 24 h. **(A)** Intracellular iron levels in 52E cells. (n = 3). **(B)** RT-PCR results of *ACSL4* in 52E cells. (n = 4). **(C)** RT-PCR results of *GPX4* in 52E cells. (n = 4). **(D)** Western blot results of GPX4 in 52E cells. (n = 3). **(E)** Changed genes in Era + QCT treated group compared with Era group displayed in volcano plot assayed by RNA-sequence. The 52E cells were treated with Era (1 μM) with or without QCT (10 μM) for 24 h. **(F)** Enrichment analysis of Kyoto Encyclopedia of Genes and Genomes (KEGG) signaling pathway in Era + QCT group compared with Era group assayed by RNA-sequence in 52E cells. **(G)** RT-PCR results of *SLC7A11, SLC3A2, ATF3, Hmox-1* in 52E cells. (n = 4). **(H) and (I)** After transfected with siRNA for 24 h, the cells were treated with Era (1 μM) for 24 h and the level of *ATF3*, *SLC7A11*, *GPX4*, lipid ROS levels, and cell viability in 52E cells were determined. (n = 4–6). $^{*}P < 0.05$, $^{**}P < 0.01$, $^{***}P < 0.001$, compared with CON group; $\#P < 0.05$, $\#\#P < 0.01$, $\#\#\#P < 0.001$, compared with Era or RSL3 group.

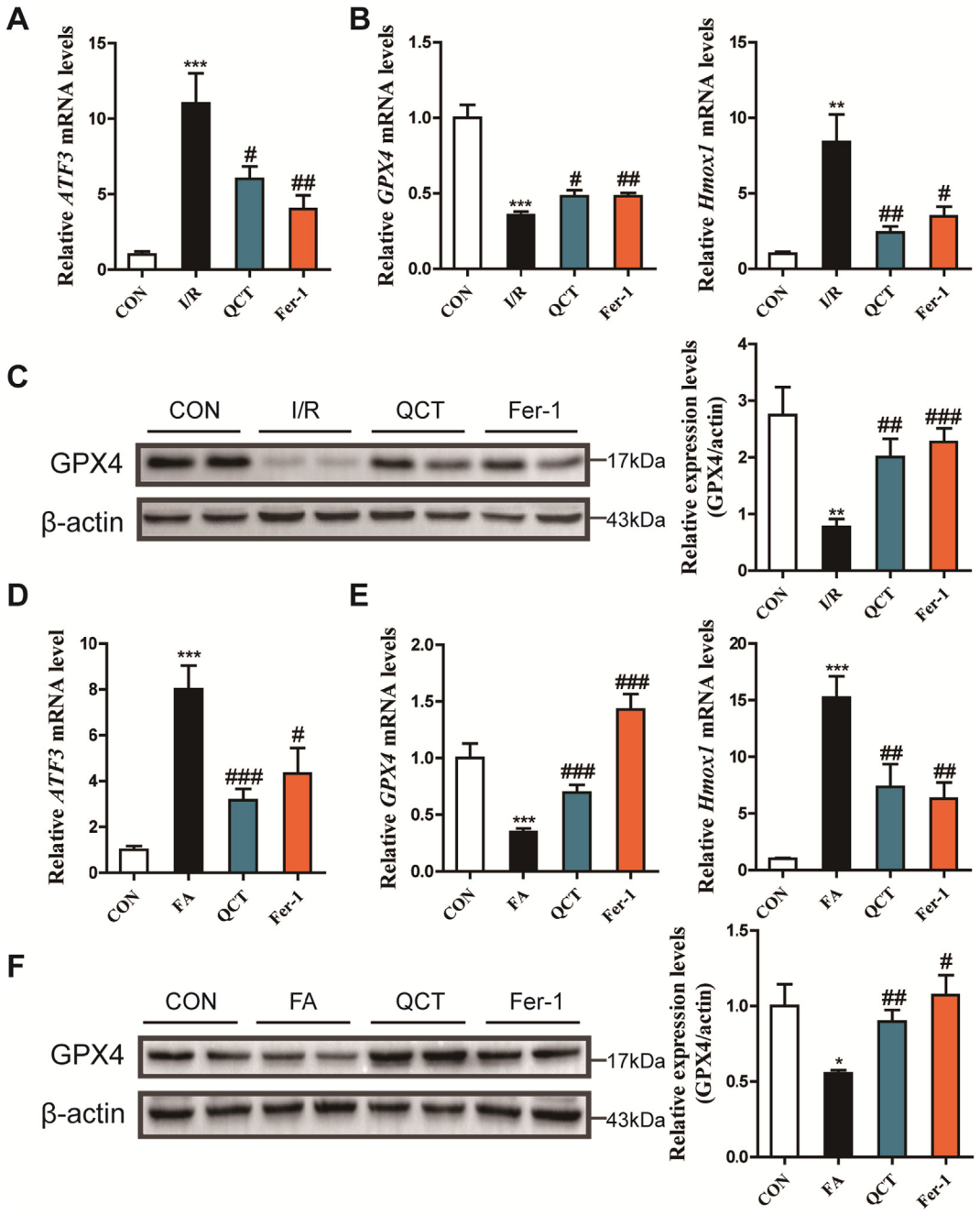


**Fig. 4.** QCT decreased ATF3 and increased GPX4 expression in AKI mice. **(A)** RT-PCR results of *ATF3* in I/R-AKI mice. **(B)** RT-PCR results of *GPX4*, *Hmox-1* in I/R-AKI mice. **(C)** Western blot results of GPX4 in I/R-AKI mice. **(D)** RT-PCR results of *ATF3* in FA-AKI mice. **(E)** RT-PCR results of *GPX4*, *Hmox-1* in FA-AKI mice. **(F)** Western blot results of GPX4 in FA-AKI mice. (n = 6). $^{*}P < 0.05$, $^{**}P < 0.01$, $^{***}P < 0.001$, compared with CON group; $\#P < 0.05$, $\#\#P < 0.01$, $\#\#\#P < 0.001$, compared with I/R or FA group.

*Ferroptotic cells induced the recruitment and chemotaxis of macrophages through CCL2*

AKI is histologically characterized by tubular cell death and inflammation. Regulated necrosis including ferroptosis is thought to be extremely pro-inflammatory and immunogenic [1]. But how ferroptosis trigger inflammation is poorly understood. Through RNA-sequence and enrichment analysis of KEGG signaling pathways in the Era group compared with the Control group of 52E cells, we found that changed genes in the Era group were enriched in inflammatory pathways, such as "response to tumor necrosis factor", "response to molecules of bacterial origin", "response to lipopolysaccharide" and "response to cytokine" (Fig. 5A). Many inflammation related genes were up-regulated by Era, such as *MMP9*, *Ptgs2*, *Lcn2* (Fig. 5B). Of note, macrophage chemokines, *CCL2* and *CCL7*, were also increased in the Era group compared with the Control group (Fig. 5B). RT-PCR results confirmed the increase of chemokines induced by Era, whereas QCT treatment significantly decreased both levels of *CCL2* and *CCL7* (Fig. 5C). To test whether ferroptotic cells could promote macrophage migration, we added 52E cells treated with Era or DMSO in the lower chamber of the transwell and iBMDMs in the upper chamber for 24 h.

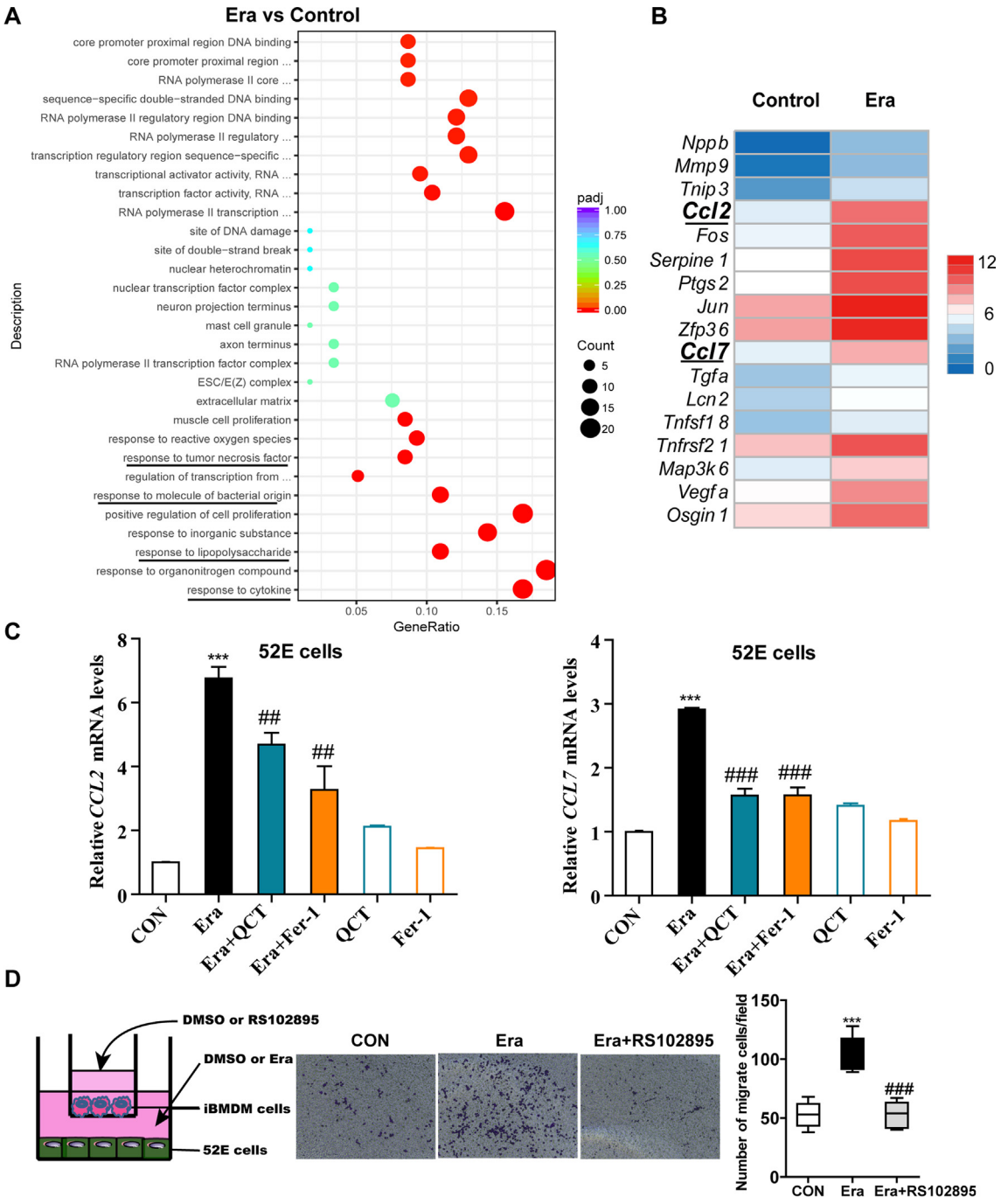


**Fig. 5.** Ferroptotic cells induced the recruitment and chemotaxis of macrophages through CCL2. **(A)** Enrichment analysis of KEGG signaling pathway in Era group compared with Control group assayed by RNA-sequence in 52E cells. **(B)** Changed inflammation-related genes in Era group compared with Control group displayed in heatmap assayed by RNA-sequence in 52E cells. **(C)** RT-PCR results of *CCL2*, *CCL7* in 52E cells after treatment for 24 h. (n = 4). **(D)** Left, iBMDM migration assay (visualized by crystal violet stain) using 52E cells treated with Era or DMSO for 24 h. Right, Quantitative analysis of the cell migration number. (n = 3). The scale bar represents 50 μm. ***$P$ < 0.001, compared with CON group; ##$P$ < 0.01, ###$P$ < 0.001, compared with Era group.

Results showed a significant increase of migrated cells by ferroptotic cells, while administration of RS102895, an inhibitor of CCR2 to the upper chamber, curtailed the migration of macrophages (Fig. 5D). In addition, Era alone without 52E cells didn't improve the migration of macrophages (Fig. S5A), and RS102895 had no influence on cell viability of iBMDMs (Fig. S5B), which excluded a non-specific effect of the drugs. Collectively, these results prove that ferroptotic cells induce a pro-inflammatory state by triggering the recruitment of macrophages through CCL2, and that QCT can inhibit ferroptosis-induced inflammation in vitro.

### *QCT diminished the inflammation in mice of AKI models*

To further confirm the pro-inflammatory effect of ferroptotic cells induced by chemotaxis of macrophages in vivo, we treated the mice with RS102895. The results showed a protective effect of RS102895 in FA-AKI, reducing kidney coefficient and blood CRE and BUN (Fig. 6A). Masson staining of kidney tissues also showed that RS102895 significantly reduced histologic injury (Fig. 6B). We further investigated the effect of QCT or Fer-1 on kidney inflammation. Infiltrated macrophages were increased in

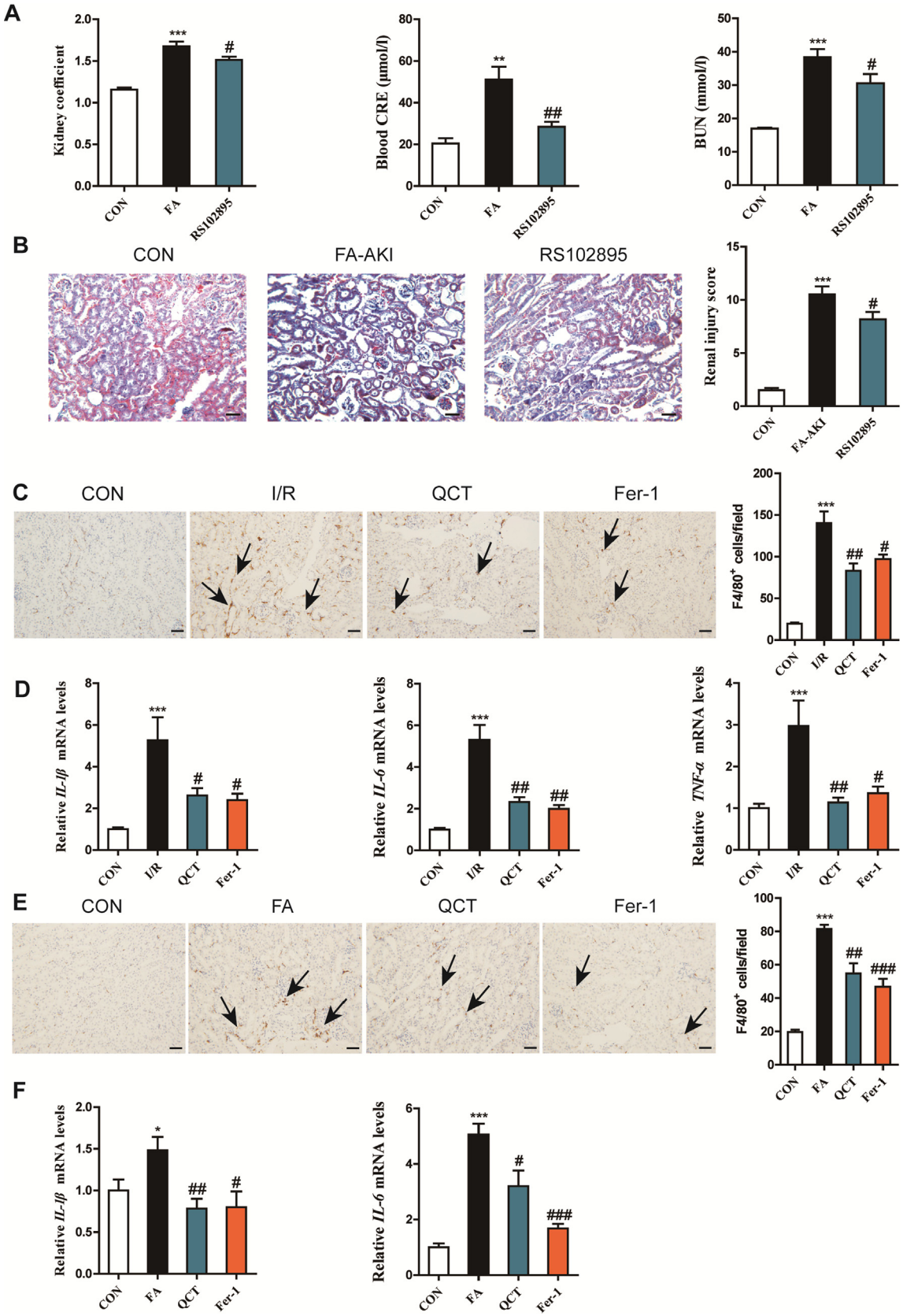


**Fig. 6.** QCT diminished the inflammation in murine AKI models. **(A)** Kidney coefficient and BUN and blood CRE levels in FA-AKI mice. (n = 6). **(B)** Representative Masson staining, and pathological scores of the kidneys in FA-AKI groups. The scale bar represents 50 μm. (n = 6). **(C)** Representative F4/80 staining photographs, and mean F4/80 positive cells in I/R-AKI mice counted in 5 fields. Black arrows indicate positive F4/80 staining cells; statistic results of $F4/80^+$ cells/field are listed on the right. The scale bar represents 50 μm. (n = 6). **(D)** RT-PCR results of *IL-1β*, *IL-6*, *TNF-α* in I/R-AKI mice. (n = 6). **(E)** Representative F4/80 staining photographs, and mean F4/80 positive cells in FA-AKI mice counted in 5 fields. Black arrows indicate positive F4/80 staining cells; statistic results of $F4/80^+$ cells/field are listed on the right. The scale bar represents 50 μm. (n = 6). **(F)** RT-PCR results of *IL-1β*, *IL-6* in FA-AKI mice. (n = 6). $^*P < 0.05$, $^{***}P < 0.001$, compared with CON group; #$P < 0.05$, ##$P < 0.01$, ###$P < 0.001$, compared with I/R or FA group.

mice of the I/R-AKI model, and were then reduced after QCT or Fer-1 administration (Fig. 6C). In addition, *IL-1β*, *IL-6* and *TNF-α* levels in kidney were reduced by QCT or Fer-1 (Fig. 6D). Consistently, upsurge of infiltrated macrophages and pro-inflammatory cytokines were also mitigated by QCT in FA-AKI (Fig. 6E, F). All these results suggest that ferroptotic cells trigger inflammation in kidney by promoting pro-inflammatory cytokine release and the recruitment of macrophages, and inhibition of ferroptosis by QCT can alleviate the inflammation-mediated kidney injury.

## Discussion

AKI is caused by factors such as kidney I/R, sepsis or nephrotoxins and is characterized by impaired kidney-filtration function. The damage of the kidney tubular epithelial cells causes loss of kidney function and increases morbidity and mortality. Unfortunately, AKI still remains a headache condition which lacks specific tools for treatment until now. Understanding the pathophysiology of one disease is always the cornerstone for exploration of novel diagnostic and therapeutic strategies. Emerging evidence supports the concept that ferroptosis, among all the types of cell death, plays critical role in the pathophysiology of AKI, highlighting ferroptosis as a promising target for treatment of AKI.

Ferroptosis is a regulated form of cell death driven by loss of activity of the lipid repair enzyme GPX4 and subsequent accumulation of lipid-based ROS. Researchers found that ferroptosis inhibitor Fer-1 prevented AKI [7,8]. N-acetylcysteine, a lipid oxidation reducer, shows a protective role in FA and star fruit-induced AKI [31,32]. Era could inhibit cystine uptake by the cystine/glutamate antiporter (system $xc^-$), and act on voltage dependent anion channels 2 and 3 (VDAC2/3), destroying the antioxidant defenses and promoting ROS production by the cell and ultimately leading to ferroptosis [3,29]. RSL3, a glutathione (GSH) peroxidase (GPX) 4 inhibitor, is another popularly used inducer of ferroptosis [3]. We found that QCT, an anti-oxidant, significantly inhibited both Era and RSL3 induced-ferroptosis, increased the cell viability and decreased cellular lipid ROS. As expected, QCT also showed as a therapeutic drug candidate for both I/R-AKI and FA-AKI, protecting from functional acute renal failure and structural organ damage. Meanwhile, lipid peroxidation in kidney tissues was blocked by QCT, consistent with previous studies that showed that QCT possessed the effect of alleviating intracellular ROS generation [33,34]. Interestingly, QCT is also a main component of "Huangkui capsule", which was proven to have wide renal protective effect and is widely used for diabetic nephropathy and other kidney diseases in China [35,36]. But the mechanisms behind "Huangkui capsule" remain poorly understood. The inhibitory effect of QCT on ferroptosis of kidney tubular epithelial cells shown here might provide the possible mechanism for "Huangkui capsule". However, QCT has poor bioavailability and solubility, which limits its application [37–39]. Also, unlike in vitro studies of QCT, the in vivo studies are more complex, considering the possible effect of its metabolites. The absorption and pharmacokinetics of QCT should be further studied. QCT in this manuscript was orally administrated 25 mg/kg for three times/day based on several exploration tests, while oral administration of QCT at 10 mg/kg daily was unable to protect against isoproterenol cardiotoxicity as reported [40]. Optimization of the structure of QCT to get a new compound with higher bioavailability and solubility is needed in further studies.

Ferroptosis is dependent upon intracellular iron, accumulation of lipid ROS, and loss of activity of the lipid repair enzyme GPX4. In the present study, no increasing iron content was found in cells developing ferroptosis or kidney tissues of AKI mice. While disruption of GPX4 was repaired by QCT, and lipid ROS was abrogated. According to the RNA-sequence analysis, we identified ATF3 as a core factor that contributed to the ferroptosis. ATF3 belongs to a member of the ATF/cyclic AMP response element-binding (ATF/CREB) family of transcription factors, considered as a stress response-inducing gene. And ATF3 was proven to be involved in various types of cell regulation, including stress response, cell cycle regulation, apoptosis and immune regulation [41]. ATF3 has also been reported to change in various diseases such as atherosclerosis [42], cardiac hypertrophy [43], breast cancer [41], colorectal cancer [44] and other tumors. Recently, ATF4, another member of ATF/CREB family of transcription factors, was found to promote angiogenesis and neuronal cell death through ferroptosis in an Xct-dependent manner [45]. Wolfram reported that high levels of ATF3 correlated with low glutathione during sepsis [46]. Recently, ATF3 was proven to promote ferroptosis [47]. We also found that ATF3 was increased in AKI, and that knockdown of ATF3 increased the cell viability of the renal proximal tubular epithelium and the expression of *GPX4*. Our data revealed that QCT could markedly inhibit ATF3 and suggested that QCT may inhibit ferroptosis through the repression of ATF3. In addition, a strong repression by QCT of Hmox-1 was also found. Hmox-1, the enzyme that is responsible for heme degradation, is upregulated in proximal tubule cells in response to oxidant stress. But its role in ferroptosis is controversial, some reported Hmox-1 mitigated ferroptosis [48], while others found Hmox-1 accelerated ferroptosis [49]. Based on our results, the effect of QCT on Hmox-1 was more likely to be accompanied by the inhibition on ferroptosis.

Besides tubular cell death, inflammation is also an important characteristic of AKI, histopathologically correlated with renal dysfunction [50]. It is known that dying cells release inflammatory factors which amplify tissue injury. Ferroptosis, together with other types of regulated necrosis, is thought to be immunogenic and extremely pro-inflammatory, but how ferroptosis causes inflammation remains poorly characterized. Through the RNA-sequence analysis, we found that molecular inflammatory pathways were activated in ferroptotic cells. Many inflammation related genes, especially macrophage chemokines CCL2 and CCL7, were triggered by ferroptosis. Ferroptotic cells did induce the recruitment of macrophages according to our experiments. Many references showed an important role of macrophages in AKI, stimulating and amplifying inflammatory responses [51,52]. QCT and Fer-1, inhibitors of ferroptosis, significantly reduced the infiltration of macrophages and levels of inflammatory cytokines in kidney. Our findings here clearly link cell death-immune crosstalk to AKI development and define important cellular and molecular mediators which may serve as effective targets in AKI.

## Conclusion

In conclusion, this study provides evidences that QCT possess a protective role on AKI via inhibiting ferroptosis. Our studies suggest that (i) QCT is a potent ferroptosis inhibitor and ameliorates AKI; (ii) QCT reduces ATF3 expression and further influences the downstream signaling pathway of ferroptosis; (iii) Ferroptosis could induce the recruitment of macrophages, triggering inflammation. We view this work as a first step toward developing treatments for AKI targeting ferroptosis, and provide the basis for the development of new therapeutic strategies for diseases related to ferroptosis.

## Compliance with Ethics Requirements

*All Institutional and National Guidelines for the care and use of animals (fisheries) were followed.*

*All animal experiments were performed in accordance with the National Institutes of Health Guide for the Care and Use of Laboratory Animals, with the approval of Center for New Drug Safety Evaluation and Research, China Pharmaceutical University. The ethical committee number for the study is B20170722-1.*

## Declaration of Competing Interest

*The authors have declared no conflict of interest.*

## Acknowledgments

This work was supported by National Natural Science Foundation of China grants, China (81603132 and 81673468) and Double First class'University project, China (no cPU2018gF10 and cPU2018gY46). It also supported in part by the Intramural Research Program of the NIH, USA (Project Z01-ES-101684 to LB).

## Author contributions

X.G., Y.W., and X.L. designed research; Y.W., F.Q., Q.C., Y.L., C.Y., R.B., H.Y., X.C. and X.G. performed research; Y.W., Q.C., X.G. and X.L. analyzed data; X.G., Y.W., L.B., and Y.Y. wrote the paper.

## Appendix A. Supplementary material

Supplementary data to this article can be found online at https://doi.org/10.1016/j.jare.2020.07.007.

## References

[1] Martin-Sanchez D, Poveda J, Fontecha-Barriuso M, Ruiz-Andres O, Sanchez-Nino MD, Ruiz-Ortega M, et al. Targeting of regulated necrosis in kidney disease. Nefrologia: publicacion oficial de la Sociedad Espanola Nefrologia 2018;38:125–35.
[2] Linkermann A, Chen G, Dong G, Kunzendorf U, Krautwald S, Dong Z. Regulated cell death in AKI. J Am Soc Nephrol: JASN 2014;25:2689–701.
[3] Dixon SJ, Lemberg KM, Lamprecht MR, Skouta R, Zaitsev EM, Gleason CE, et al. Ferroptosis: an iron-dependent form of nonapoptotic cell death. Cell 2012;149:1060–72.
[4] Xie Y, Hou W, Song X, Yu Y, Huang J, Sun X, et al. Ferroptosis: process and function. Cell Death Differ 2016;23:369–79.
[5] Friedmann Angeli JP, Schneider M, Proneth B, Tyurina YY, Tyurin VA, Hammond VJ, et al. Inactivation of the ferroptosis regulator Gpx4 triggers acute renal failure in mice. Nat Cell Biol 2014;16:1180–91.
[6] Yang WS, SriRamaratnam R, Welsch ME, Shimada K, Skouta R, Viswanathan VS, et al. Regulation of ferroptotic cancer cell death by GPX4. Cell 2014;156:317–31.
[7] Linkermann A, Skouta R, Himmerkus N, Mulay SR, Dewitz C, De Zen F, et al. Synchronized renal tubular cell death involves ferroptosis. Proc Nat Acad Sci USA 2014;111:16836–41.
[8] Martin-Sanchez D, Ruiz-Andres O, Poveda J, Carrasco S, Cannata-Ortiz P, Sanchez-Nino MD, et al. Ferroptosis, but not necroptosis, is important in nephrotoxic folic acid-induced AKI. J Am Soc Nephrol: JASN 2017;28:218–29.
[9] Skouta R, Dixon SJ, Wang J, Dunn DE, Orman M, Shimada K, et al. Ferrostatins inhibit oxidative lipid damage and cell death in diverse disease models. J Am Chem Soc 2014;136:4551–6.
[10] Patel RV, Mistry BM, Shinde SK, Syed R, Singh V, Shin HS. Therapeutic potential of quercetin as a cardiovascular agent. Eur J Med Chem 2018;155:889–904.
[11] Rauf A, Imran M, Khan IA, Ur-Rehman M, Gilani SA, Mehmood Z, et al. Anticancer potential of quercetin: A comprehensive review. Phytotherapy Res: PTR 2018.
[12] Cui S, Wu Q, Wang J, Li M, Qian J, Li S. Quercetin inhibits LPS-induced macrophage migration by suppressing the iNOS/FAK/paxillin pathway and modulating the cytoskeleton. Cell Adhes Migrat 2018:1–12.
[13] Pathak S, Regmi S, Nguyen TT, Gupta B, Gautam M, Yong CS, et al. Polymeric microsphere-facilitated site-specific delivery of quercetin prevents senescence of pancreatic islets in vivo and improves transplantation outcomes in mouse model of diabetes. Acta Biomater 2018.
[14] Zhu Y, Tchkonia T, Pirtskhalava T, Gower AC, Ding H, Giorgadze N, et al. The Achilles' heel of senescent cells: from transcriptome to senolytic drugs. Aging Cell 2015;14:644–58.
[15] Xu M, Pirtskhalava T, Farr JN, Weigand BM, Palmer AK, Weivoda MM, et al. Senolytics improve physical function and increase lifespan in old age. Nat Med 2018;24:1246–56.
[16] Gomes IB, Porto ML, Santos MC, Campagnaro BP, Gava AL, Meyrelles SS, et al. The protective effects of oral low-dose quercetin on diabetic nephropathy in hypercholesterolemic mice. Front Physiol 2015;6:247.
[17] Lesjak M, Hoque R, Balesaria S, Skinner V, Debnam ES, Srai SK, et al. Quercetin inhibits intestinal iron absorption and ferroportin transporter expression in vivo and in vitro. PLoS ONE 2014;9:e102900.
[18] Cheng IF, Breen K. On the ability of four flavonoids, baicilein, luteolin, naringenin, and quercetin, to suppress the Fenton reaction of the iron-ATP complex. Biomet: Int J Role Met Ions Biol, Biochem, Med 2000;13:77–83.
[19] Li X, Zeng J, Liu Y, Liang M, Liu Q, Li Z, et al. Inhibitory effect and mechanism of action of quercetin and quercetin diels-alder anti-dimer on erastin-induced ferroptosis in bone marrow-derived mesenchymal stem cells. Antioxidants 2020:9.
[20] Vichai V, Kirtikara K. Sulforhodamine B colorimetric assay for cytotoxicity screening. Nat Protoc 2006;1:1112–6.
[21] Lien EC, Lyssiotis CA, Juvekar A, Hu H, Asara JM, Cantley LC, et al. Glutathione biosynthesis is a metabolic vulnerability in PI(3)K/Akt-driven breast cancer. Nat Cell Biol 2016;18:572–8.
[22] Lu B, Chen XB, Hong YC, Zhu H, He QJ, Yang B, et al. Identification of PRDX6 as a regulator of ferroptosis. Acta Pharmacol Sin 2019;40:1334–42.
[23] Doll S, Freitas FP, Shah R, Aldrovandi M, da Silva MC, Ingold I, et al. FSP1 is a glutathione-independent ferroptosis suppressor. Nature 2019;575:693–8.
[24] Brooks C, Wei Q, Cho SG, Dong Z. Regulation of mitochondrial dynamics in acute kidney injury in cell culture and rodent models. J Clin Investig 2009;119:1275–85.
[25] Menke J, Iwata Y, Rabacal WA, Basu R, Yeung YG, Humphreys BD, et al. CSF-1 signals directly to renal tubular epithelial cells to mediate repair in mice. J Clin Investig 2009;119:2330–42.
[26] Wei Q, Yin XM, Wang MH, Dong Z. Bid deficiency ameliorates ischemic renal failure and delays animal death in C57BL/6 mice. Am J Physiol Renal Physiol 2006;290:F35–42.
[27] Perfettini JL, Roumier T, Kroemer G. Mitochondrial fusion and fission in the control of apoptosis. Trends Cell Biol 2005;15:179–83.
[28] Song X, Zhu S, Chen P, Hou W, Wen Q, Liu J, et al. AMPK-mediated BECN1 phosphorylation promotes ferroptosis by directly blocking system Xc(-) activity. Current Biol: CB 2018;28(2388–99):e5.
[29] Yagoda N, von Rechenberg M, Zaganjor E, Bauer AJ, Yang WS, Fridman DJ, et al. RAS-RAF-MEK-dependent oxidative cell death involving voltage-dependent anion channels. Nature 2007;447:864–8.
[30] Doll S, Proneth B, Tyurina YY, Panzilius E, Kobayashi S, Ingold I, et al. ACSL4 dictates ferroptosis sensitivity by shaping cellular lipid composition. Nat Chem Biol 2017;13:91–8.
[31] Shimizu MH, Gois PH, Volpini RA, Canale D, Luchi WM, Froeder L, et al. N-acetylcysteine protects against star fruit-induced acute kidney injury. Ren Fail 2017;39:193–202.
[32] Wang HZ, Peng ZY, Wen XY, Rimmele T, Bishop JV, Kellum JA. N-acetylcysteine is effective for prevention but not for treatment of folic acid-induced acute kidney injury in mice. Crit Care Med 2011;39:2487–94.
[33] Li Y, Zhou S, Li J, Sun Y, Hasimu H, Liu R, et al. Quercetin protects human brain microvascular endothelial cells from fibrillar beta-amyloid1-40-induced toxicity. Acta Pharm Sinica B 2015;5:47–54.
[34] Yao P, Nussler A, Liu L, Hao L, Song F, Schirmeier A, et al. Quercetin protects human hepatocytes from ethanol-derived oxidative stress by inducing heme oxygenase-1 via the MAPK/Nrf2 pathways. J Hepatol 2007;47:253–61.
[35] Yang X, Luo M, Jiang Q, Wang Y. Effects of Huangkui capsule on the expression of SPARC in the kidney tissue of a rat model with diabetic nephropathy. Curr Gene Ther 2019.
[36] Cai HD, Su SL, Qian DW, Guo S, Tao WW, Cong XD, et al. Renal protective effect and action mechanism of Huangkui capsule and its main five flavonoids. J Ethnopharmacol 2017;206:152–9.
[37] Chen X, Yin OQ, Zuo Z, Chow MS. Pharmacokinetics and modeling of quercetin and metabolites. Pharm Res 2005;22:892–901.
[38] Rechner AR, Kuhnle G, Hu H, Roedig-Penman A, van den Braak MH, Moore KP, et al. The metabolism of dietary polyphenols and the relevance to circulating levels of conjugated metabolites. Free Radical Res 2002;36:1229–41.
[39] Rothwell JA, Urpi-Sarda M, Boto-Ordonez M, Llorach R, Farran-Codina A, Barupal DK, et al. Systematic analysis of the polyphenol metabolome using the Phenol-Explorer database. Mol Nutr Food Res 2016;60:203–11.
[40] Riha M, Voprsalova M, Pilarova V, Semecky V, Holeckova M, Vavrova J, et al. Oral administration of quercetin is unable to protect against isoproterenol cardiotoxicity. Naunyn-Schmiedeberg's Arch Pharmacol 2014;387:823–35.
[41] Yin X, Dewille JW, Hai T. A potential dichotomous role of ATF3, an adaptive-response gene, in cancer development. Oncogene 2008;27:2118–27.
[42] Gold ES, Ramsey SA, Sartain MJ, Selinummi J, Podolsky I, Rodriguez DJ, et al. ATF3 protects against atherosclerosis by suppressing 25-hydroxycholesterol-induced lipid body formation. J Exp Med 2012;209:807–17.
[43] Zhou H, Guo H, Zong J, Dai J, Yuan Y, Bian ZY, et al. ATF3 regulates multiple targets and may play a dual role in cardiac hypertrophy and injury. Int J Cardiol 2014;174:838–9.
[44] Bottone Jr FG, Moon Y, Kim JS, Alston-Mills B, Ishibashi M, Eling TE. The anti-invasive activity of cyclooxygenase inhibitors is regulated by the transcription factor ATF3 (activating transcription factor 3). Mol Cancer Ther 2005;4:693–703.
[45] Chen D, Fan Z, Rauh M, Buchfelder M, Eyupoglu IY, Savaskan N. ATF4 promotes angiogenesis and neuronal cell death and confers ferroptosis in a xCT-dependent manner. Oncogene 2017;36:5593–608.

[46] Hoetzenecker W, Echtenacher B, Guenova E, Hoetzenecker K, Woelbing F, Bruck J, et al. ROS-induced ATF3 causes susceptibility to secondary infections during sepsis-associated immunosuppression. Nat Med 2011;18:128–34.
[47] Wang L, Liu Y, Du T, Yang H, Lei L, Guo M, et al. ATF3 promotes erastin-induced ferroptosis by suppressing system Xc–. Cell Death Differ 2019.
[48] Adedoyin O, Boddu R, Traylor A, Lever JM, Bolisetty S, George JF, et al. Heme oxygenase-1 mitigates ferroptosis in renal proximal tubule cells. Am J Physiol Renal Physiol 2018;314:F702–14.
[49] Kwon MY, Park E, Lee SJ, Chung SW. Heme oxygenase-1 accelerates erastin-induced ferroptotic cell death. Oncotarget 2015;6:24393–403.
[50] Gonzalez-Guerrero C, Cannata-Ortiz P, Guerri C, Egido J, Ortiz A, Ramos AM. TLR4-mediated inflammation is a key pathogenic event leading to kidney damage and fibrosis in cyclosporine nephrotoxicity. Arch Toxicol 2017;91:1925–39.
[51] Djudjaj S, Martin IV, Buhl EM, Nothofer NJ, Leng L, Piecychna M, et al. Macrophage migration inhibitory factor limits renal inflammation and fibrosis by counteracting tubular cell cycle arrest. J Am Soc Nephrol: JASN 2017;28:3590–604.
[52] Lv LL, Feng Y, Wen Y, Wu WJ, Ni HF, Li ZL, et al. Exosomal CCL2 from tubular epithelial cells is critical for albumin-induced tubulointerstitial inflammation. J Am Soc Nephrol: JASN 2018;29:919–35.